07

Modification of AlGaN/GaN transistor structure parameters by passivation and hydrogen plasma treatment

© A.V. Kovalchuk,[1] V.E. Zemlyakov,[2] S.I. Karcev,[2] D.S. Shpakov,[2] S.Yu. Shapoval[1]

[1] Institute of Microelectronics Technology and High-Purity Materials
142432 Chernogolovka, Moscow Region, Russia
[2] National Research University „Moscow Research Institute of Electronic Technology" (MIET),
124498 Moscow, Russia
e-mail: anatoly-fizmat@mail.ru

Received May 8, 2025
Revised August 7, 2025
Accepted August 14, 2025

Efficiency of passivation of AlGaN/GaN transistor structures by low-temperature silicon nitride, $H_xSi_rN_zH_y$, is demonstrated. Significant increase in the slope of current-voltage curve, saturation current and power-added efficiency is shown. Effective bulk hydrogenation process of $H_xSi_rN_zH_y$ /AlGaN/GaN transistor structures was developed and includes: modification of charge states in the volume of $H_xSi_rN_zH_y$ and states associated with the $H_xSi_rN_zH_y$ /AlGaN interface, and hydrogen atom passivation of point defects of the crystalline structure in the epitaxial AlGaN and GaN layers. Silicon nitride passivation and hydrogenation processes were developed on the basis of an electron cyclotron resonance plasma technology. Hydrogenation process is an effective and simple solution for compensation of negative thermal destruction (depassivation) processes occurring at ($> 600\,^{\circ}$C) stages in the AlGaN high electron mobility transistor process cycle.

Keywords: AlGaN HEMTs, 2DEG, electron cyclotron resonance, ECR plasma, trap state passivation, silicon nitride, semiconductor structure hydrogenation.

DOI: 10.61011/TP.2026.02.62887.109-25

Introduction

It has been reported earlier that silicon nitride passivation of AlGaN HEMTs (High Electron Mobility Transistors) on the basis of undoped heterostructures, where two-dimensional electron gas (2DEG) was formed by means of polarization, made it possible to avoid the current collapse effect [1]. Strong electric polarization, which is present in undoped pseudomorphic $Al_xGa_{1-x}N$/GaN structures grown at the Ga facet induces 2DEG with a surface density about $1 \cdot 10^{13}\,\mathrm{cm}^{-2}$ at $0.3 < x < 0.4$ [2]. This undoped structure has some advantages over doped HEMT structures. High electron mobility, noise lower by several orders of magnitude $1/f$ and lower electric field under the gate for channel stop condition achievement are among them [2]. Nevertheless charge carrier trap effects (unoccupied bulk dislocation states and/or surface-related states) lead to current drop during high voltage or pulsed operation [1,2]. Silicon nitride passivation is widely used to reduce electron tunneling in the 2DEG region to states related to the heterostructure surface.

Results of plasma-chemical vapor deposition of silicon nitride in high frequency plasma process (chemical vapour deposition (CVD)) [3] and electron cyclotron resonance plasma process (ECR) [1] were reported. Silicon nitride passivation of transistor structures is used to improve their output characteristics. This can be explained either by hydrogen passivation of electrically-active centers or by the effect of positive charge occurring in silicon nitride containing hydrogen bonds, or by both.

Later, positive results of performance improvement of transistor structures on the basis of doped AlGaN epitaxial structures using various techniques and passivating layer materials were reported. They include silicon nitride passivation in inductively coupled plasma [4]; the use of silicon nitride thick films deposited by the LPCVD (Low Pressure Chemical Vapor Deposition) technique [5]; catalysis [6]; *in-situ* passivation [7]; the use of organic materials [8]; silicon dioxide films [9,10]; aluminum oxide layers [11]; aluminum nitride [12,13]; aluminum nitride and hafnium oxide [14]; AlTiO layers [15].

All listed methods provide significant improvement of transistor structure parameters. However, in the authors' opinion, the effect of hydrogen dissolved in (Van der Waals-bound) in the grown AlGaN epitaxial structures and the effect of hydrogen bonds in the passivating layer and at the $H_xSi_rN_zH_y$/AlGaN interface shall be considered. This hydrogen influences trap state energy levels. Therefore a change in the concentration of dissolved hydrogen and of chemically-bound hydrogen shall be taken into account in the transistor structure manufacturing process.

At the same time AlGaN/GaN-based structures and other solid solution structures are usually formed as heterostructures on substrates made of other materials (silicon, silicon carbide, sapphire, etc), as a result these structures have a high threading dislocation density up to $10^7-10^{11}\,\mathrm{cm}^{-2}$ due to substantial mismatch of lattices, thermal stresses and

other parameters [16–19]. Regions with high density of defects having acceptor-consistent properties are formed around the dislocation core. Of course, this leads to charge carrier scattering and recombination [20–24], degradation of transistor structure properties (saturation current, leakage current, current collapse, noise level, radiation resistance, etc.) [25–30]. However, electronic structures on the basis of third group nitrides can have outstanding properties with a dislocation density, as mentioned above, many orders of magnitude higher that the dislocation density in silicon, gallium arsenide structures and many others [31,32]. A mechanism behind this phenomenon is still not fully understood.

Vacancies are experimentally detected by a positron annihilation method [19,33–35]. These results show that Ga vacancies are present in concentrations of $10^{17}-10^{18}\,\mathrm{cm}^{-3}$ in undoped bulk crystals and GaN layers, while Mg-doped samples are free from Ga vacancies. Ga vacancies are negatively charged and their concentration correlates with yellow luminescence band intensity. Ga vacancies probably facilitate electrical compensation of *n*-type GaN, and their acceptor levels participate in generation of the yellow luminescence band.

Direct observation of vacancies uses the direct real-space visualization on a cleaved GaN surface via atomic force microscopy and scanning tunneling microscopy [36].

Calculations using ab initio methods [37,38] show that hydrogen can compensate a vacancy, giving up an electron to the acceptor level, and passivate a vacancy, forming a hydrogen–vacancy complex [37]. It has been shown recently on the basis of ab initio calculations that deep states can be also removed from edge dislocations via oxygen passivation after GaN crystal growth [39].

At the same time, investigation of vacancies using the positron annihilation and atomic force microscopy techniques involve considerable impact on samples due to the presence of high energy particles and possible noticeable mechanical damage and, consequently, excitation of mechanical stress in a crystal structure. And ab initio calculations can lead to considerable deviations from experimental data [37,38,40].

Therefore, approaches to investigation of vacancies in third group nitrides using yellow band luminescence [41] and capacitance-voltage characteristics using deep level transient spectroscopy (DLTS) may turn out to be promising [42].

In epitaxial gallium nitride structures, high hydrogen concentration is detected after epitaxy [42–44]. This can facilitate preservation of high electrophysical properties of transistor structures because hydrogen can passivate p-type impurities and defects in third group nitrides, this effect is observed up to annealing temperatures of 800 °C.

However, annealing at temperatures above 900 °C leads to removal of hydrogen from *p*-type gallium nitride [44] and slightly reduces the hydrogen concentration in *n*-type gallium nitride. Hydrogen has low solubility in *n*-type structures. Hydrogen easily diffuses into *p*-type gallium nitride, but hydrogen diffusion into *n*-type gallium nitride or through GaN:Mg/GaN:Si type structures is considerably weakened. These phenomena are accounted for by the fact that hydrogen is negatively charged in *n*-type GaN and positively charged in *p*-type GaN or high-resistance GaN [43].

Similarly in passivating silicon nitride, hydrogen is quickly removed via high-temperature annealing, for example, it is shown that the time of hydrogen diffusion escape from a 100 nm silicon nitride layer at 800 K is $2.1 \cdot 10^{-5}$ s [45].

The foregoing suggests that hydrogen contained in epitaxial gallium nitride actively reacts with electrically-active centers in the epitaxial structure and passivating silicon nitride, influencing to a significant extent on electron transport in transistor structures. However, when epitaxial structures are exposed to heat during transistor structure manufacturing process (for example, contact baking), hydrogen concentration both within the epitaxial structures and in the passivating silicon nitride (at the dielectric–semiconductor interface) significantly decreases. This can lead to a change in transistor structure properties, reduction of saturation current and power output, increase in leakage, etc.

There are known techniques allowing hydrogen introduction into bulk GaN/AlGaN heterostructures using radio-frequency deuterium plasma [30]. Substrate was treated in deuterium plasma at 260 °C during 10 min. In this case, deuterium concentration of $10^{17}-10^{21}\,\mathrm{cm}^{-3}$ was reached at depths of 1–100 nm.

This led to an increase in a set of transistor structure parameters such as saturation current, leakage current and, consequently, dynamic characteristics by 10 %–30 %. In addition, note that hydrogen processing can facilitate halogen radical removal from the third group nitride volume after traditional semiconductor structure manufacturing processes [46].

The authors examine the efficiency of passivating silicon nitride deposition on the transistor structure surface and the effect of hydrogen plasma processing at the end of the process on the electrical parameters of transistor structures.

1. Experimental setup

Hydrogenation of AlGaN/GaN transistor structures and passivation by plasma-chemical silicon nitride, $H_xSi_rN_zH_y$, were performed on a microwave plasma generation unit in electron cyclotron resonance (ECR) conditions. The laboratory-assembled unit makes it possible to change and maintain the absorbed microwave power and to control the energy of N_2^+, N^+, Si^+, H_2^+ and H^+ protons. Energies of ions and protons striking the surface of a sample were varied by a negative bias potential U_b, which ranged from a floating potential V_{flo} [47] to −160 V.

The diagram of the experimental setup is shown in Figure 1. Charge was generated by absorption of magnetron microwave power in the ECR chamber (diameter 15 cm,

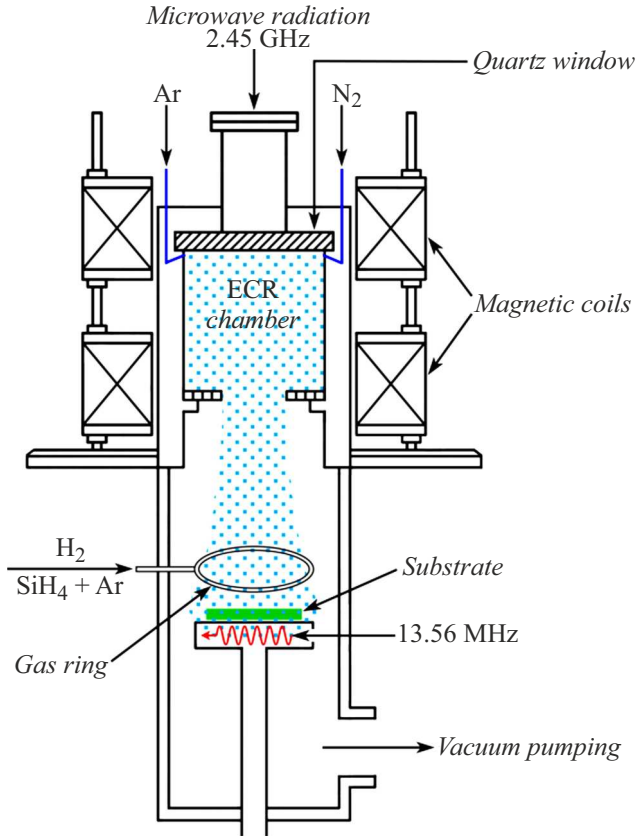

Figure 1. Diagram of the experimental setup with plasma charge generation in ECR conditions: microwave radiation frequency $f = 2.45$ GHz, resonance magnetic field $B_r = 875$ G. Microwave energy flux arrives into the ECR chamber(diameter Ø = 15 cm, length $L = 16$ cm) via a microwave path consisting of rectangular-profile waveguides. To control the energy of positively charged ions, HF voltage with controlled amplitude is applied to the substrate holder (Si, SiC or Al_2O_3 wafer with transistor structures). The setup can be used both for passivation and hydrogenation of AlGaN/GaN transistor structures. Gas ring is used to arrange homogeneous molecular flow distribution of the active gas on substrate surface (SiH_4 or H_2). Gas mixture ($1 \cdot SiH_4 + 3 \cdot Ar$) and coaxial inleakage of N_2 to the ECR chamber are used for passivation. Hydrogenation uses H_2 and coaxial inleakage of Ar to the ECR chamber. Coaxially symmetric inleakage of N_2 or Ar is arranged from the cylinder periphery at the ECR chamber inlet so that the molecular flows „slide" along the quartz window surface to center.

length 16 cm). Microwave power W_{in} emitted by a magnetron tube at $f = 2.45$ GHz can be stably maintained by a generator within $W_{in} = 50-1000$ W. Microwave energy flux arrives into the ECR chamber via the microwave path consisting of rectangular-profile waveguides. An automatic tuner is used for impedance matching and minimization of reflected power W_{ref}.

Optimum distribution of magnetic field induction within the ECR chamber is achieved by moving magnetic coils parallel to the chamber along the rod guides. Thus, magnetic field $B_r = 875$ G, which is necessary to maintain ECR conditions, is achieved at a distance of 40 mm from the quartz window (Figure 1) and later remains unchanged at a length of 30 mm along the ECR chamber axis.

For hydrogenation of transistor structures, the plasma was held in a hydrogen and argon mixture. Argon was fed coaxially symmetrically from the quartz window periphery at the ECR chamber inlet. For passivation, Ar was replaced with N_2 (Figure 1). The wafer with AlGaN/Ga transistor structures was placed in a substrate holder located coaxially at a distance of 120 mm from the ECR chamber outlet. To generate U_b, 13.56 MHz HF voltage with a controlled amplitude was applied to the substrate holder with respect to the ECR plasma unit.

The optimum conditions for ECR plasma treatment were selected by varying the substrate temperature T=40 °C−300 °C, microwave power W=50−400 W, pressure $P = 0.1-4$ mTorr, and the ratio $R = 0.2-1.0$ of H_2/Ar flows. For passivation, the optimum ratio of SiH_4/N_2 flows was kept equal to 1.05.

Far from the ECR region and chamber walls in plasma $\{e, N_2^+\}$, the electron energy is $kT_e \approx 5$ eV. The electron flux in any direction is ≈ 1000 times higher than the ion flux. This is due to the mass ratio ($M_i/m_e \approx 51\,000$) and temperature ratio ($T_e/T_i \approx 20$) of the electron and ion components of neutral plasma. Isolated substrate placed in the plasma region will receive a negative charge necessary for flattening electron and ion fluxes on its surface. With respect to neutral plasma, the substrate will be charged by the negative potential. Such potential in plasma physics is called the floating potential V_{flo}. In plasma $\{e, N_2^+\}$, $V_{flo} \approx -5.155 \cdot kT_e \approx -26$ V [47].

Physical pattern is modified, if HF voltage is fed to the substrate with respect to the chamber walls as shown in Figure 1. Under the action of a force pulse from the HF field, electron gas cloud displacement is M_i/m_e times greater than that of the ion array. In each plasma oscillation period, the substrate is „immersed" in the electron cloud. Plasma polarization will occur near the substrate surface. As a result of such polarization, the negative charge layer will move to the substrate surface, and the positive charge layer will be distributed at a distance from the substrate surface. With respect to the neutral plasma, the substrate receives the negative potential U_b, the magnitude of which is defined by the HF field amplitude. Positive ions in the particle flux striking the substrate surface pass via the polarization region and acquire an energy equal to eU_b. For more detailed description of the rectifying action of near-electrode plasma on the HF field, see the book by Yu.P. Raizer [48].

Due to high degree of ionization (0.001−0.1) in the ECR plasma conditions, sufficient fluxes of active particles are provided to maintain the processes of homogeneous film deposition on the substrate [49] at chamber pressures of $(0.1-10) \cdot 10^{-3}$ Torr.

2. Findings

2.1. Study of plasma-chemical silicon nitride $H_x Si_r N_z H_y$

Due to the known advantages of the ECR plasma [49,50], the silicon nitride layer deposition process was performed in an ECR plasma unit. Thus, to avoid possible defect formation, we aimed to reduce the ion energy and simultaneously to increase the electron gas density (degree of plasma discharge ionization).

Deposition process optimization is driven by a significant difference between the chemical formula $Si_3N_4$and the atomic composition of the real material of the ${}_xSi_rN_zH_y$ layer, which is called „silicon nitride“ in microelectronic technology. Molecular formula $H_xSi_rN_zH_y$ for silicon nitride was introduced in [45]. In this formula, x, r, z, y are atomic percentages. $x + r + z + y = 100\,\%$; $x = C(\mathrm{Si{-}H})$, $r = C(\mathrm{Si})$, $z = C(\mathrm{N})$, $y = C(\mathrm{N{-}H})$. Percentages of hydrogen atoms x and y depend on the „silicon nitride“ deposition process and temperature. The minimum amount $x + y = 5\%$ can be achieved via high temperature ($T > 1200\,\mathrm{K}$) pyrolytic layer deposition. The total percentage of hydrogen atoms in low-temperature ($T < 600\,\mathrm{K}$) plasma-chemical layer deposition can be as high as 38 % [51].

Thus, the „silicon nitride“ layer, $H_xSi_rN_zH_y$, is a polymer-like material and initially contains chemically bound (≡Si−H, =N−H) hydrogen atoms. AlGaN HEMTs were passivated by $H_xSi_rN_zH_y$ in conditions providing approximately equal concentrations ($x \approx y = 14\,\%$) of Si−H and N−H bonds.

$H_xSi_rN_zH_y$ layers (1000 Å) were deposited from nitrogen and monosilane (SiH_4) diluted with argon (1:3). Substrate temperature 200 °C and SiH_4/N_2 flow ratio were varied within (0.75−1.25), pressure was 3 mTorr, absorbed microwave power was $(W_{in} - W_{ref}) = 200\,\mathrm{W}$.

To study the properties of silicon nitride, $H_xSi_rN_zH_y$ layers were deposited onto high-resistance Si (111) wafers (p-type, 10 Ω·cm). The refractive index of silicon nitride was varied within 1.96−2.03 by changing the SiH_4/N_2 flow ratio (0.9−1.1). Figure 2 shows the FTIR (Fourier Transform Infrared Spectroscopy) spectrum of the $H_xSi_rN_zH_y$ layer with the base peak $\nu_o = 838\,\mathrm{cm}^{-1}$ normalized to the absorbance $A = 1$. The amount of included hydrogen and type of chemical bond were determined by absorption peaks of the Si−H stretching modes at $2180\,\mathrm{cm}^{-1}$ and N−H at $3340\,\mathrm{cm}^{-1}$.

FTIR spectra were scanned using the Bruker VERTEX 27 V Fourier research IR spectrometer. All spectra were recorded with the resolution $\Delta\nu = 4\,\mathrm{cm}^{-1}$ in the wavenumber range from 370 cm-1 to $6370\,\mathrm{cm}^{-1}$ with accumulation and automatic averaging of 625 scans. In Grams/386 (Thermo Fisher Scientific corporation), Ir spectrum of high-resistance {Si (111)} was subtracted from $\{H_xSi_rN_zH_y + \mathrm{Si}\,(111)\}$. Then the differential IR spectrum $\{H_xSi_rN_zH_y\}$ was reduced to the form of ANIRS (Absolute

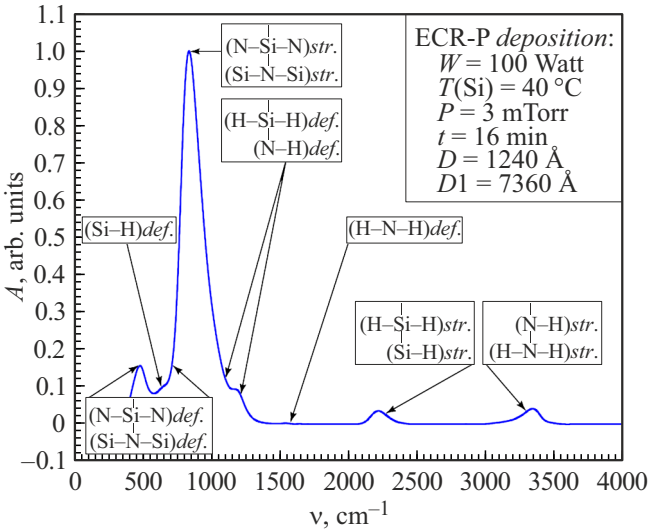

Figure 2. FTIR spectrum of plasma-chemical silicon nitride $H_xSi_rN_zH_y$ ($x + r + z + y = 100$). Spectrum is shown with the base peak $\nu_o = 838\,\mathrm{cm}^{-1}$ normalized to the absorbance $A = 1$ (10-fold fall of intensity of transmitted IR radiation). Layer thickness $D_1 = 7360$ Å corresponds to $A = 1$.

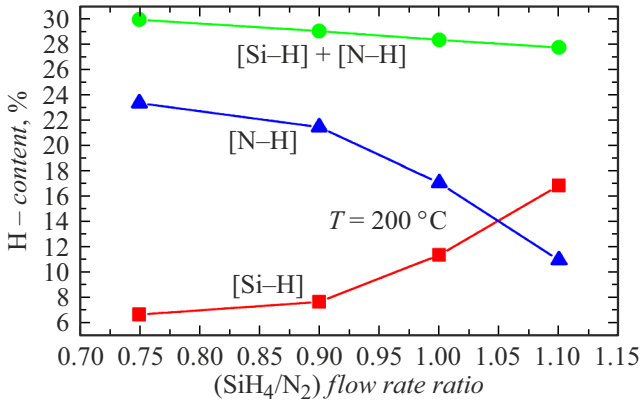

Figure 3. Concentration of hydrogen in the plasma-chemical $H_xSi_rN_zH_y$ ($x + r + z + y = 100$) layers depending on the SiH_4/N_2 flow ratio.

Normalized Infrared Spectrum) in Grams/386, as shown in Figure 2. It is the IR spectrum reduced to ANIRS that is suitable for analysis and mathematical processing. Procedure of reducing the differential IR spectrum $\{H_xSi_rN_zH_y\}$ to ANIRS is described in detail in [51].

In [51], we have developed a mathematical tool designed to use the IR Fourier spectroscopy for calculating the atomic composition (x, r, z, y) in $H_xSi_rN_zH_y$ layers with a submicron thickness of 500−3000 Å. Concentration of hydrogen in $H_xSi_rN_zH_y$ layers depending on the SiH_4/N_2 flow ratio is shown in Figure 3. At a deposition temperature of 200 °C for percentages of Si−H and N−H, there were sharp changes with small deviations of (SiH_4/N_2) near 1.05. The total concentration of hydrogen was almost constant (Figure 3). At $(SiH_4/N_2) = 1.05$ and

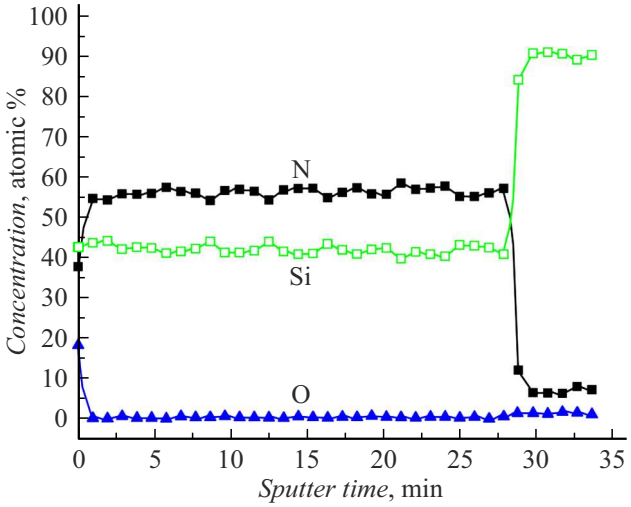

Figure 4. Distribution of O, Si, N concentrations by the plasma-chemical $H_xSi_rN_zH_y$ $(x + r + z + y = 100)$ layer thickness measured using SIMS.

a deposition temperature of 200 °C, equal concentration of Si−H and N−H is achieved in $H_xSi_rN_zH_y$ so that $x = y \approx 14\,\%$ and $r/z = 3/4$ as is the case for stoichiometric Si_3N_4. This means that a pair of (H,H) atoms is chemically built into each dangling bond $(Si-\cdots-N) :\Rightarrow (H,H) + (Si-\cdots-N) = Si-H + N-H$. A local potential energy minimum is apparently reached in the $H_xSi_rN_zH_y$ structure at $x = y$.

Figure 4 shows the SIMS (secondary ion mass-spectrometry) measurements of atomic concentrations. Concentrations of Si, N, O atoms in the silicon nitride layer depth measured using the SIMS technique were almost constant. SIMS spectra were measured on the TOF.SIMS-5 (IONTOF, Germany) secondary ion mass-spectrometer with an ultimate sensitivity of 10^{14} atoms/cm^3. Measurements were performed at $5 \cdot 10^{-5}$ Pa in dynamic mode. Silicon nitride sputtering rate was ≈ 50 Å/min. Primary ion energy Xe^+ was equal to 1 keV.

2.2. Passivation of AlGaN HEMTs by plasma-chemical silicon nitride $H_xSi_rN_zH_y$

Transistor structures are test field-effect transistors made on a AlGaN/GaN heterostructure grown on a sapphire substrate, with Ti/Al/Ni/Au resistance contacts and Ni/Au gate, and passivated by plasma-chemical $H_xSi_rN_zH_y$.

Saturation currents, output power and power-added efficiency before and after passivation were measured for undoped AlGaN/GaN on transistor structures with a $2 \times 37.5 \times 0.3\,\mu$m gate. Measurements were performed at 10 GHz ($V_{ds} = 15$ V, $V_{gs} = -3.8$ V). Increase in the output power up to 40 % was achieved. Figure 5 shows the output power and power-added efficiency (PAE) before and after passivation.

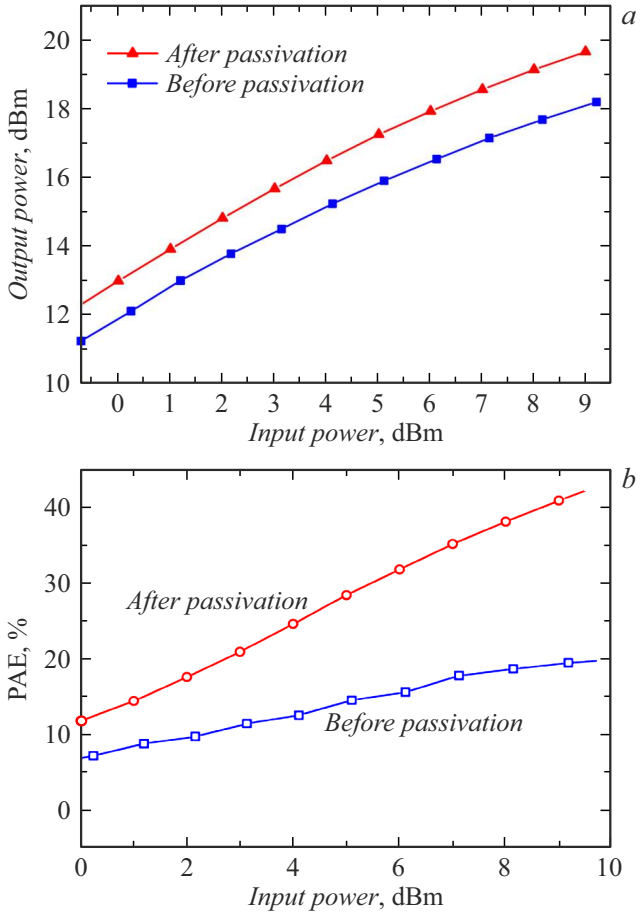

Figure 5. Output power (a) and PAE (b) before and after passivation of AlGaN/GaN HEMT. Measurements were made at 10 GHz.

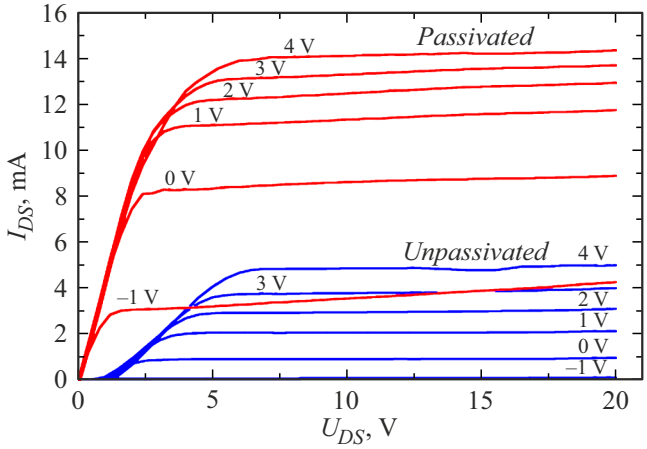

Figure 6. Current-voltage (I–V) curves of AlGaN/GaN transistors before and after passivation by $H_xSi_rN_zH_y$. Gate dimensions - $2 \times 50 \times 0.3\,\mu$m. Maximum gate voltage - $V_g = +4$ V. Characteristics are written at $V_g = 1$ V intervals.

As can be seen in Figure 6, the slope of the current-voltage curve and saturation current have increased signif-

icantly. There is an increase in PAE from 20 % to 41 % after passivation. It is clear from these measurements that passivation strongly reduces the depletion of the conductivity channel region under the gate–drain semiconductor surface, which leads to more pronounced possibility for active channel modulation.

2.3. Influence of hydrogen plasma treatment on saturation currents and leakage currents of transistor structures

Transistor structure samples with identical geometry were processed in hydrogen ($H_2 + Ar$) ECR plasma at a pressure of 2 mTorr, flow ratio $F(H_2)/F(Ar) = 1$, absorbed microwave power $(W_{in} - W_{ref}) = 300$ W, self-bias potential $U_b = -120$ V and various exposure times. Substrate holder temperature was 200 °C.

A group of wafers with similar transistor structures was placed on the surface of a mirror-finished stainless steel table, to which HF voltage with controlled amplitude was applied (Figure 1). After five-minute hydrogen ECR plasma treatment and process termination, a part of wafers were removed from the reactor. Other wafers remained on the substrate holder surface for adding the next five-minute treatment portion. And so on, until 25 min treatment was reached for the last pair of wafers. Such procedure was used to avoid significant adiabatic heating of a wafer in gas discharge plasma, if the wafer is continuously treated during 25 min. At 2 mTorr, the wafer temperature can significantly deviate from 200 °C due to the Knudsen heat transfer in the gas interlayer between the wafer and mirror-finished table. It is important that such technique allowed addition of identical five-minute treatment portions for further experimental points. Proton flux accelerated by U_b is transformed into a hydrogen atom flow. Individual temperature of each wafer is a critical hydrogenation parameter

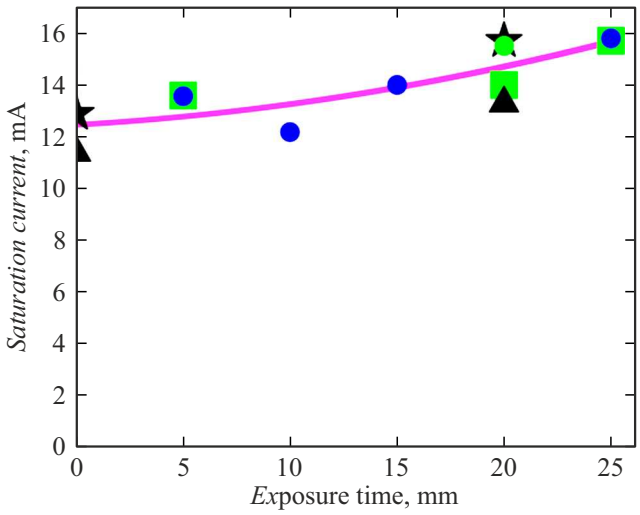

Figure 7. Dependence of saturation current on ECR hydrogen plasma treatment time of AlGaN/GaN transistor structures with a gate $2 \times 50 \times 0.3\,\mu$m, $V_g = +4$ V.

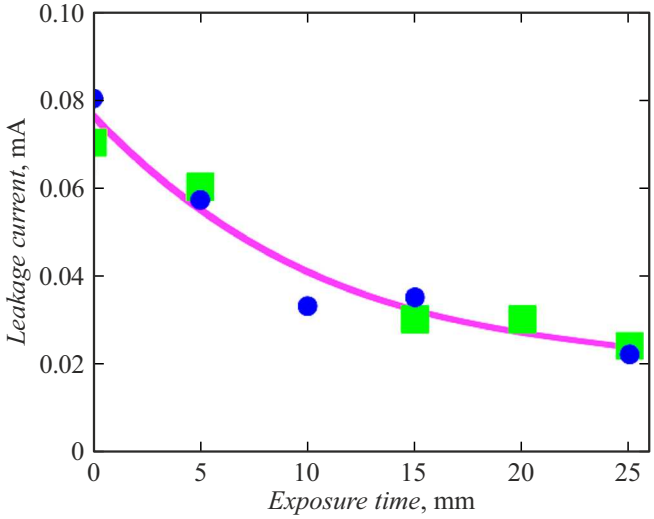

Figure 8. Dependence of leakage current on ECR hydrogen plasma treatment time of AlGaN/GaN transistor structures with a gate $2 \times 50 \times 0.3\,\mu$m, $V_g = +4$ V.

because the process of hydrogen atom penetration into deep transistor layers (≈ 100 nm) is of diffusion nature.

Figure 7, 8 shows that both currents (saturation and leakage) are significantly dependent on the plasma treatment time. This can suggest that hydrogen diffuses into the heterostructure volume and passivates acceptors not only on the surface, but also in the semiconductor volume [21].

Conclusion

Grown epitaxial AlGaN/GaN structures contain hydrogen with concentration comparable (or higher) with that of n-type or p-type structures.

Hydrogen can escape from the epitaxial structure volume during heat treatments, thus reducing the concentration to a much lower level than that of electrically-active centers.

Atomic hydrogen localized near the epitaxial structure surface can probably passivate trap states on the epitaxial structure surface, preventing electron tunneling from the two-dimensional gas region to surface traps and a change in the two-dimensional electron gas density.

At the same time, during ECR hydrogen plasma treatment, hydrogen diffuses into the epitaxial structure volume, reducing the free hole concentration. And ultimately it can lead to an increase in saturation current, output power and power-added efficiency of transistor structures at least with an undoped channel.

Not so vivid, but substantial dependence of transistor saturation current and leakage currents on hydrogen plasma treatment time can suggest that during treatment hydrogen diffuses into the heterostructure volume and passivates acceptors not only on the surface, but also in the semiconductor volume.

Our conclusion that hydrogen saturation at low temperatures and at the end of electronic device formation processes coincides with conclusions of [39] that oxygen inclusion during growth can be harmful; it becomes useful, if it takes place at the cooling or postgrowth heat treatment phase at much lower temperature. This may be indicative of some common hydrogen and oxygen binding mechanisms in the presence of vacancies and dislocations.

Funding

The study was performed within the framework of the topic of the state order of the Institute of Microelectronics Technology RAS: STATE TASK № 075-00295-25-00.

Conflict of interest

The authors declare no conflict of interest.

References

[1] S. Shapoval, V. Gurtovoi, A. Kovalchuk, L. Eastman, A. Vertjachih, C. Gaquiere, D. Theron. *Proc. of „WOCSDICE-2002 — XXVI Workshop on Compound Semiconductor Devices and Integrated Circuits“* (Chernogolovka, Russia, 2002), p. VII.7.

[2] L.F. Eastman. *Proc. of „WOCSDICE-2000 — XXIV Workshop on Compound Semiconductor Devices and Integrated Circuits“* (Aegean Sea, Greece, 2000), p. VIII-7.

[3] C. Gaquiere, B. Boudart, R. Amokrane, Y. Crosnier, J.C. De jaeger, F. Omnes. *Proc. of „WOCSDICE-2000 — XXIV Workshop on Compound Semiconductor Devices and Integrated Circuits“* (Aegean Sea, Greece, 2000), p. VIII-11.

[4] A.A. Sleptsova, S.V. Chernykh, D.A. Podgorny, I.A. Zhilnikov. Modern Electron. Mater., **6** (2), 71 (2020). https://doi.org/10.3897/j.moem.6.2.58860

[5] X. Wang, S. Huang, Y. Zheng, K. Wei, X. Chen, G. Liu, T. Yuan, W. Luo, L. Pang, H. Jiang, H. Robust. IEEE Electron. Device Lett., **36** (7), 666 (2015). DOI: 10.1109/LED.2015.2432039_https://ieeexplore.ieee.org/document/7105867

[6] S. Okada, H. Matsumura. Jpn. J. Appl. Phys., **36** (11R), 7035 (1997). DOI: 10.1143/JJAP.36.7035_ https://iopscience.iop.org/article/10.1143/JJAP.36.7035

[7] K.N. Tomosh, A.Yu. Pavlov, V.Yu. Pavlov, R.A. Khabibullin, S.S. Arutyunyan, P.P. Maltsev. Semiconductors, **50** (10), 1434 (2016). https://doi.org/10.1134/S1063782616100225

[8] Manjari Garg, Tejas Rajendra Naik, Ravi Pathak, Valipe Ramgopal Rao, Che-Hao Liao, Kuang-Hui Li, Haiding, Sun, Xiaohang Li, Rajendra Singh. J. Appl. Phys., **124**, 195702 (2018). https://doi.org/10.1063/1.5049873

[9] P. Javorka, J. Bernat, A. Fox, M. Marso, H. Lüth, P. Kordoš. Electron. Lett., **39**, 1155 (2003). https://doi.org/10.1049/el:20030748

[10] S. Arulkumaran, T. Egawa, H. Ishikawa, T. Jimbo, Y. Sano. Appl. Phys. Lett., **84**, 613 (2004). https://doi.org/10.1063/1.1642276

[11] D. Xu, K. Chu, J. Diaz, W. Zhu, R. Roy, L.M. Pleasant, K. Nichols, P.-C. Chao, M. Xu, D.Y. Peide. IEEE Electron. Device Lett., **34** (6), 744 (2013). https://doi.org/10.1109/LED.2013.2255257

[12] S. Huang, Q. Jiang, S. Yang, C. Zhou, K.L. Chen. IEEE Electron. Device Lett., **33** (4), 516 (2012). DOI: 10.1109/LED.2012.2185921_https://ieeexplore.ieee.org/document/6155727

[13] Z. Tang, S. Huang, Q. Jiang, S. Liu, C. Liu, K.J. Chen. IEEE Electron Device Lett., **34** (3), 366 (2013). DOI: 10.1109/LED.2012.2236638_https://ieeexplore.ieee.org/document/6410341

[14] Zikri Zulkifli, Norshamsuri Ali, Shaili Falina, Hiroshi Kawarada, Mohamed Fauzi Packeer Mohamed, Mohd Syamsul. Key Eng. Mater., **947**, 21 (2023). https://doi.org/10.4028/p-445y05

[15] Sayak Dutta Gupta, Rajarshi Roy Chaudhuri, Mayank Shrivastava. IEEE Transactions on Electron Devices, **68** (11), 5728 (2021). https://doi.org/10.1109/TED.2021.3064531

[16] Zhi-Yu Lin, Zhi-Bin Chen, Jin-Cheng Zhang, Sheng-Rui Xu, Teng Jiang, Jun Luo, Li-Xin Guo, Yue Hao. Chin. Phys. Lett., **35** (2), 026104 (2018). https://cpl.iphy.ac.cn/article/doi/10.1088/0256-307X/35/2/026104

[17] A. Pandey, B.S. Yadav, D.V.S. Rao, D. Kaur, A.K. Kapoor. Appl. Phys. A., **122**, 614 (2016). DOI: 10.1007/s00339-016-0143-3_https://link.springer.com/article/10.1007/s00339-016-0143-3

[18] P. Kumar, S. Rao, J. Lee, D. Singh, R.K. Singh. J. Solid State Sc. Tech., **2** (1), P1 (2012). DOI: 10.1149/2.009301jss_ https://iopscience.iop.org/article/10.1149/2.009301jss

[19] J. Oila, J. Kiviola, V. Ranki, K. Saarinen, D.C. Look, R.J. Molnar, S.S. Park, S.K. Lee, J.Y. Han. Appl. Phys. Lett., **82**, 3433 (2003). https://doi.org/10.1063/1.1569414

[20] J. Elsner, R. Jones, P.K. Sitch, V.D. Porezag, M. Elstner, Th. Frauenheim, M.I. Heggie, S. Öberg, P.R. Briddon. Phys. Rev. Lett., **79**, 3672 (1997). https://doi.org/10.1103/PhysRevLett.79.3672

[21] U. Jahn, O. Brandt, E. Luna, X. Sun, H. Wang, D.S. Jiang, L.F. Bian, H. Yang. Phys. Rev. B, **81**, 125314 (2010). http://dx.doi.org/10.1103/PhysRevB.81.125314

[22] J. Cai, F.A. Ponce. Phys. Stat. Sol. A, **192**, 407 (2002). https://doi.org/10.1002/1521-396X(200208)192:2¡407::AID-PSSA407¿3.0.CO;2-M

[23] E. Muller, D. Gerthsen, P. Brückner, E. Scholz, Th. Gruber, A. Waag. Phys. Rev. B, **73**, 245316 (2006). https://doi.org/10.1103/PhysRevB.73.245316

[24] J. Yu, Z. Hao, L. Li, L. Wang, Y. Luo, J. Wang, Ch. Sun, Y. Han, B. Xiong, H. Li. AIP Adv., **7**, 035321 (2017). https://doi.org/10.1063/1.4979504

[25] K. Qiu, X.H. Li, Z.J. Yin, X.C. Cao, Q.F. Han, C.H. Duan, X.J. Zhou, M. Liu, T.F. Shi, X.D. Luo, Y.Q. Wang. EPL, **82**, 18002 (2008). https://doi.org/10.1209/0295-5075/82/18002

[26] J.H. You, J.Q. Lu, H.T. Johnson. J. Appl. Phys., **99** (3), 033706 (2006). https://doi.org/10.1063/1.2168028

[27] E.C.H. Kyle, S.W. Kaun, P.G. Burke, F. Wu, Y.R. Wu, J.S. Speck. J. Appl. Phys., **115** (19), 193702 (2014). https://doi.org/10.1063/1.4874735

[28] S. Besendörfer, E. Meissner, A. Lesnik, J. Friedrich, A. Dadgar, T. Erlbacher. J. Appl. Phys., **125** (9), 095704 (2019). https://doi.org/10.1063/1.5065442

[29] M. Tapajna, S.W. Kaun, M.H. Wong, F. Gao, T. Palacios, U.K. Mishra, J.S. Speck, M. Kuball. Appl. Phys. Lett., **99** (22), 223501 (2011). https://doi.org/10.1063/1.3663573
[30] J. Mimila-Arroyo, E. Morales, A. Lusson, J.M. Laroche, F. Jomard, M. Tessier. Superficies y Vacío, **23** (4), 31 (2010). http://www.redalyc.org/articulo.oa?id=94216142007
[31] S. Lester, F. Ponce, M. Craford, D. Steigerwald. Appl. Phys. Lett., **66** (10), 1249 (1995). https://doi.org/10.1063/1.113252
[32] T.D. Moustakas. Phys. Status Solidi A, **210** (1), 169 (2013). https://doi.org/10.1002/pssa.201200561
[33] A. Uedono, K. Tenjinbayashi, T. Tsutsui, Y. Shimahara, H. Miyake, K. Hiramatsu, N. Oshima, R. Suzuki, S. Ishibashi. J. Appl. Phys., **111** (1), 013512 (2012). https://doi.org/10.1063/1.3675270
[34] K. Saarinen, T. Laine, S. Kuisma, J. Nissilä, P. Hautojärvi, L. Dobrzynski, J.M. Baranowski, K. Pakula, R. Stepniewski, M. Wojdak, A. Wysmolek, T. Suski, M. Leszczynski, I. Grzegory, S. Porowski. Phys. Rev. Lett., **79**, 3030 (1997). https://doi.org/10.1103/PhysRevLett.79.3030
[35] V. Prozheeva, I. Makkonen, H. Li, S. Keller, U.K. Mishra, F. Tuomisto. Phys. Rev. Appl., **13**, 044034 (2020). https://doi.org/10.1103/PhysRevApplied.13.044034
[36] Keisuke Sagisaka, Oscar Custance, Nobuyuki Ishida, Tomonori Nakamura, Yasuo Koide. Phys. Rev. B, **106**, 115309 (2022). https://doi.org/10.1103/PhysRevB.106.115309
[37] A.F. Wright. J. Appl. Phys., **90** (3), 1164 (2001). https://doi.org/10.1063/1.1383980
[38] J.P. Perdew, A. Zunger. Phys. Rev. B, **23**, 5048 (1981). https://doi.org/10.1103/PhysRevB.23.5048
[39] Sayre Christenson, Weiyu Xie, Yi-Yang Sun, S.B. Zhang. Phys. Rev. B, **95**, 121201 (2017). DOI: 10.1103/PhysRevB.95.121201_https://link.aps.org/accepted/10.1103/PhysRevB.95.121201
[40] Su-Huai Wie, A. Zunger. Appl. Phys. Lett., **69** (18), 2719 (1996). https://doi.org/10.1063/1.117689
[41] J. Neugebauer, Ch.G. van de Walle. Appl. Phys. Lett., **69** (4), 503 (1996). https://doi.org/10.1063/1.117767
[42] C.H. Seager, S.M. Myers, A.F. Wright, D.D. Koleske, A.A. Allerman. J. Appl. Phys., **92** (12), 7246 (2002). https://doi.org/10.1063/1.1520719
[43] R. Czernecki, E. Grzanka, R. Jakieła, S. Grzanka. J. Alloys Compounds, **747**, 354 (2018). https://doi.org/10.1016/j.jallcom.2018.02.270
[44] R. Jakiela, A. Barcz. arXiv: Materials Science, Preprint (2020). https://doi.org/10.48550/arXiv.2007.04144
[45] A. Kovalchuk, G. Beshkov, S. Shapoval. J. Res. Phys., **31** (1), 37 (2007). https://www.researchgate.net/publication/277125029
[46] S. Chen, Y. Lu, R. Kometani, K. Ishikawa, H. Kondo, Y. Tokuda, Makoto Sekine, M. Hori. AIP Advances, **2** (2), 022149 (2012). https://doi.org/10.1063/1.4729448
[47] Yu.P. Rajzer. *Fizika gazovogo razryada* (Nauka, Fizmatlit, M., 1992), gl.**8**, § 5, p. 5.3, s. 199 (in Russian). https://studizba.com/files/show/djvu/2107-1-rayzer-yu-p– fizika-gazovogo-razryada.html (in Russian)
[48] Yu.P. Rajzer. *Fizika gazovogo razryada* (Nauka, Fizmatlit, M., 1992), gl.**8**, § 4, p. 4.3, s. 479 (in Russian). https://studizba.com/files/show/djvu/2107-1-rayzer-yu-p– fizika-gazovogo-razryada.html (in Russian)
[49] S.Y. Shapoval, V.T. Petrashov, O.A. Popov, M.D. Yoder Jr., P.D. Maciel, C.K.C. Lok. J. Vac. Sci. Technol. A, **9** (6), 3071 (1991). https://doi.org/10.1116/1.577175
[50] E. Polushkin, S. Nefed'ev, A. Kovalchuk, O. Soltanovich, S. Shapoval. Rus. Microelectronics, **52** (3), 195 (2023). https://doi.org/10.1134/S1063739723700373
[51] A.V. Kovalchuk, S.U. Shapoval, S.S. Lebedev, S.A. Steblin, A.V. Volosov, N.I. Kargin. Vestnik Natsionalnogo issledovatelskogo jadernogo universiteta „MIFI", in Russian, **3** (2), 189 (2014). DOI: 10.1134/S2304487-X14020126_https://elibrary.ru/item.asp?doi=10.1134/S2304487X14020126

Translated by E.Ilyinskaya